DRAFT Measuring $\mathrm{B}(\pi^0 \to \mathrm{e}^+\mathrm{e}^-\gamma)/\mathrm{B}(\pi^0 \to \gamma\gamma)$ using $K_L \to 3\pi^0$

DRAFT

Erin Abouzaid

Enrico Fermi Institute, University of Chicago

(Dated: October 21, 2006)

INTRODUCTION

The PDG value of the branching fraction for the π^0 Dalitz decay is $\frac{\Gamma(e^+e^-\gamma)}{\Gamma(2\gamma)} = (1.213 \pm .030)\%$. It has a 2.5% uncertainty, and it is based on three measurements, the most recent of which is 25 years old.

$$(1.25 \pm .04)\% \text{ Schardt 1981, } \pi^- p \to n\pi^0 \text{ [1]}$$
$$(1.166 \pm .047)\% \text{ Samios 1961, 3071 events, } \pi^- p \to n\pi^0 \text{ [2]}$$
$$(1.17 \pm .15)\% \text{ Budagov 1960, 27 events [3]}$$

We find 66,432 $K_L \to 3\pi_d^0$ decays in KTeV data, and normalize to $K_L \to 3\pi^0$ (of which we find 3,530,309) to extract $\frac{B(\pi^0 \to e^+e^-\gamma)}{B(\pi^0 \to \gamma\gamma)} = (1.1539 \pm 0.0045 \pm 0.0152)\%$ (preliminary). The statistical error is 0.39% and the systematic error is 1.32%, giving a total relative uncertainty of 1.38%.

DATA SAMPLES

The signal mode is $K_L \to 3\pi^0$ with one π^0 decaying to $e^+e^-\gamma$ and the remaining 2 π^0s each decaying to $\gamma\gamma$, denoted $K_L \to 3\pi_d^0$, and the normalization mode is $K_L \to 3\pi^0 \to 6\gamma$. Ideally, both signal and normalization samples would come from the same trigger to reduce systematic errors associated with relative trigger inefficiencies. However, the only trigger that would have been suitable for this, trigger 6, requires exactly 6 clusters at level 3, while Dalitz decays produce 7 clusters in the calorimeter. Thus, trigger 6 (with a hardware prescale of 5, and an analysis prescale of 10) is used for $K_L \to 3\pi^0$, the normalization mode. Trigger 14, which requires 7 or more hardware clusters, is used for $K_L \to 3\pi_d^0$. Trigger definitions are given below.

Trigger6 = SPILL * ET_NEUT * VETO_NEUT * !CA * HCC_GE6

Trigger14 = SPILL * 2V * DC12 * ET_NEUT * VETO_CHRG * !HA_PION * !CA * HCC_GE7 * 1HCY

Both triggers require good spills, a minimum amount of energy in the calorimeter (ET_NEUT) and a maximum amount of energy deposited in the collar anti (CA). Trigger 6 requires the neutral veto, and trigger 14 requires the charged veto. These are defined below. Trigger 14 requires two hits in one view and one hit in the other for the VV′ banks

(2V), hits in three of four drift chamber views (DC12), less than 3 MIPS in the hadron anti (HA_PION), and that there are one or more hits in every y view (1HCY).

VETO_NEUT = !SA2 * !SA3 * !SA4 * !CIA * !REG * !HA_NEUT

VETO_CHRG = !SA2 * !SA3 * !SA4 * !CIA * !REG * !MU2

The neutral threshold for the hadron anti (HA_NEUT) is 14 MIPS.

EVENT SELECTION AND ANALYSIS

For the normalization mode, we are looking for 3 π^0s, each of which produces 2 photons. The six clusters in the calorimeter are input to KTPAIRS to determine the best pairing of the 15 possible pairings. (There are 6! ways to order the photons, but the order of each pair does not matter, so divide by 2 for each pair, and the order of the 3 pairs does not matter, so divide by 3! to get $\frac{6!}{8\times 6} = 15$.) This is done by looping over all possible pairings and calculating the z-positions of the three pions, assuming the pion mass. The z distance between each pion decay and the calorimeter is calculated by assuming the photons have a small opening angle, which allows us to use:

$$Z_{CSI} = \frac{\sqrt{E_1 E_2 r_{12}^2}}{m_{\pi^0}}$$

where E_1 and E_2 are the photon cluster energies in the calorimeter and r_{12} is the distance between the photon clusters at the calorimeter.

For each pairing, a χ^2 is formed based on the three reconstructed pion z-positions and their weighted average. The best pairing is the one which has the smallest pairing χ^2. The distance between the calorimeter and the reconstructed kaon vertex position is then the average z associated with the best pairing. To get the distance from the target to the kaon vertex (since the target is the origin in our reference frame), we subtract the vertex distance to the CSI (Z_{CSI}) from the mean depth of the photon shower in the CSI. This reconstructed kaon vertex position allows us to construct the four-momenta of the six photons, from which we reconstruct the $3\pi^0$ invariant mass.

For the signal mode, we require 7 hardware clusters in the CSI and 2 reconstructed tracks. After determining which clusters correspond to the 2 tracks, the remaining 5 'neutral' clusters are input to KTPAIRS to determine the best pairing of those 5 clusters into 2 $\pi^0 s$. (Again, there are 15 possible pairings, since there are now 5! ways to order the photons,

but the order within the 2 pairs does not matter nor does the order of the 2 pairs, so we have $\frac{5!}{4\times 2} = 15$.) The z-distances from the calorimeter are calculated for each pairing, and a pairing χ^2 is formed for each combination using the two pion z-distances. The pairing which minimizes this χ^2 is chosen, and the corresponding z-position is the reconstructed kaon vertex position, just as in the normalization mode. The neutral cluster which does not belong to either pair is tagged as the photon coming from the π^0_d decay.

This Dalitz photon is combined with the 2 tracks to form the π^0_d. The 4-momenta of the tracks combined with the 4-momentum of the Dalitz photon give the reconstructed π^0_d mass. The vertex of the 2 tracks gives another measure of the reconstructed vertex position. Since the tracks generally have a small opening angle and are therefore not very well-separated in the drift chambers, the uncertainty on the track vertex z-position is large compared to the uncertainty on the reconstructed kaon z based on the neutral clusters. The $3\pi^0_d$ mass is reconstructed using the reconstructed 4-momenta of the 2 tracks and the 5 photons; the track 4-momenta use the reconstructed z from the tracks, while the photon 4-momenta use the neutral z.

After reconstruction, the final data samples are selected using the criteria listed in Table I, and described below. For quantities that exist in both signal and normalization modes, selection requirements are as similar as possible so that uncertainties associated with making the cuts largely cancel in the ratio of the two modes. This is confirmed by varying these cuts in both modes and seeing that the ratio of branching ratios does not change significantly. For requirements on quantities appearing only in the charged (signal) mode, we vary the cut to see that the Monte Carlo (MC) matches the data well in the region of the cut.

The reconstructed vertex position is required to be between 123 and 158 meters, so that it is downstream of the mask (at 122 m) and upstream of the vacuum window (at 158.9 m). The reconstructed kaon energy must be between 40 and 160 GeV. The reconstructed $3\pi^0$ and $3\pi^0_d$ masses are required to be within about 7 MeV/c^2 of the PDG value of the kaon mass, 497.6 MeV/c^2. Both the pairing χ^2 cut and, in the Dalitz case, the cut on the reconstructed $e^+e^-\gamma$ mass (within 20 MeV/c^2 of the π^0_d mass), are designed to reduce cases of mispairing, since mispairing of the photons causes large pairing χ^2s and/or misreconstruction of the π^0 mass. The shape χ^2 is a measure of how close a cluster's transverse energy profile is to the expected transverse energy distribution for a photon shower. Thus, requiring the shape χ^2 to be less than 100 helps discriminate between clusters that 'look like' photons, which we

Quantity	Selection Criteria
Both Modes	Cut Window
$3\pi^0$, $3\pi^0_d$ Mass (GeV/c^2)	(0.490, 0.505)
Reconstructed vertex position (m)	(123.0, 158.0)
Reconstructed Kaon Energy (GeV)	(40.0, 160.)
Pairing χ^2	(0.0, 75.0)
Shape χ^2	(0.0, 100.0)
Min. Cluster Energy (GeV)	(3.0, ∞)
Min. Cluster Distance (m)	(0.075, ∞)
Ring Number (cm^2)	(0.0, 110.0)
Max. Seed Ring	(0.0, 19.0)
Min. Small Ring	(4.0, ∞)
Dalitz Only	Cut Window
$e^+e^-\gamma$ Mass (GeV/c^2)	(0.115, 0.155)
Min. Track Momentum (GeV/c)	(4.0, ∞)
Track E/P	(0.9, ∞)
Vertex χ^2	(0.0, 100.0)
Brem-γ Dist at CSI (m)	(0.01,∞)
Cell Separation (cells)	(3.0, ∞)

TABLE I: Selection criteria for signal and normalization mode.

want, and hadronic clusters, which we don't. Each cluster must be greater than 3 GeV in energy, and each track in the signal mode must be greater than 4 GeV/c in momentum. Each pair of clusters must be separated by at least 7.5 cm at the calorimeter (this is the minimum cluster distance cut in Table I) to reduce the amount of overlap between clusters. I reject events in which any of the clusters are centered on a CSI block at the outer edge of the calorimeter or directly around either of the two beam holes since a large fraction of the energy from those clusters would not be contained in the calorimeter. These are, respectively, the maximum seed ring and minimum small ring cuts in Table I. Additionally, the reconstructed center of energy has to be within the area of one of the beams at the CSI.

(This is the ring number cut variable in Table I, which gives the area in cm^2 of the smallest square that includes the center of energy and that is centered on the nearest beam.)

For Dalitz mode, there were additional selection criteria having to do with tracking. Both tracks were required to have energy to momentum ratios ($\frac{E}{P}$) greater than 0.9, since we have calibrated such that the $\frac{E}{P}$ of electrons should be centered at 1. The vertex χ^2 is calculated from the vertex position in x and y with the hypothesis that the tracks came from the same z position. Cutting on the vertex χ^2 throws out misreconstructed tracks. To reduce the number of events in which one of the electrons emits a bremsstrahlung photon as it bends in the magnet, we require that none of the seven clusters used to reconstruct $3\pi^0_d$ be found within 1 cm of the place on the CSI pointed to by either upstream track segment. The final selection criteria is the cell separation requirement. This cut requires that the tracks be separated by more than 3 cells at the first and second drift chambers. Each cell is 6.35 mm, so the distance requirement is around 2 cm. Although this cut throws away $\sim \frac{2}{3}$ of the Dalitz events that are left after all other cuts are made, it is necessary because the tracking efficiency is not well-understood for close tracks. For well-separated tracks, we can take advantage of tracking efficiency studies that have been done for the recent V_{us} analysis [4]. Although these studies were done on 97 $\pi^+\pi^-\pi^0$ data, we have redone them for the 99 sample. We have also demonstrated that the tracking loss is mainly due to accidentals in 99 (due to the higher beam intensity), and thus, largely affects pion and electron tracks in the same fashion. Details of these tracking inefficiency studies are in the Systematics section of this paper. Finally, all events are also required to pass the level one trigger verification for their respective triggers.

Reconstructed mass plots in Figure 1 and 2 show the signal in the Dalitz and $3\pi^0$ modes, respectively. In each plot, all cuts have been applied except the cut on the quantity plotted.

DATA SAMPLE INTEGRITY

Since I am using two different triggers for the analysis, I need to be sure that I am using the same runs and spills for both signal and normalization modes. Some runs and spills were lost for one mode during the split; others were lost during tape migration. These runs and spills were removed from both samples.

I performed a check on the remaining samples by comparing the run-by-run ratios of $3\pi^0$

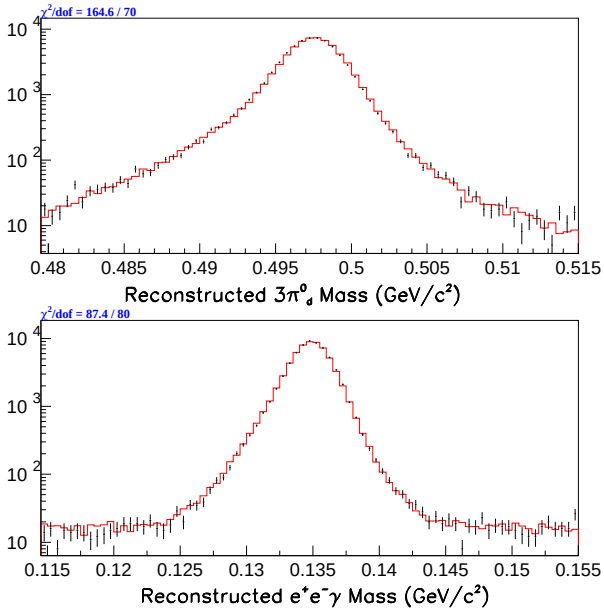

FIG. 1: The top plot is the reconstructed $3\pi^0_d$ mass and the bottom plot is the reconstructed $e^+e^-\gamma$ mass in the signal mode. The black dots are data, and the red histogram is MC. All cuts have been applied except the cut on the quantity plotted.

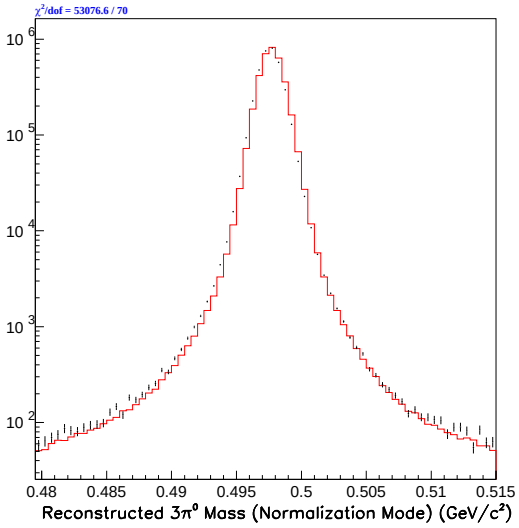

FIG. 2: The reconstructed $3\pi^0$ mass in the normalization mode. The black dots are data, and the red histogram is MC. All cuts have been applied except the cut on the reconstructed $3\pi^0$ mass.

events to Dalitz events to the average of this ratio over all runs. I looked for individual

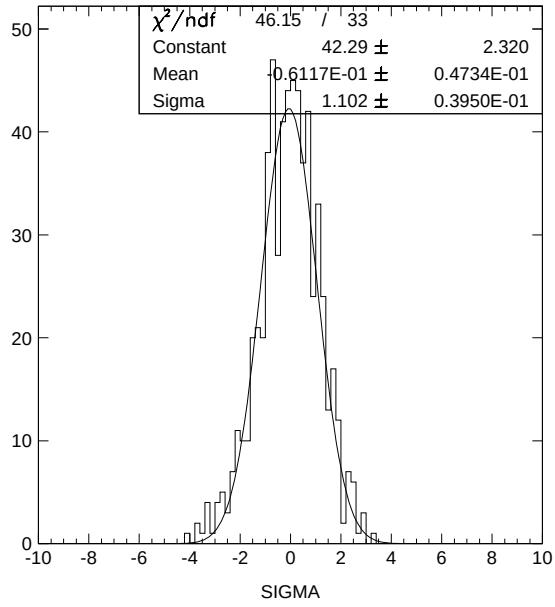

FIG. 3: The sigma distribution, fit to a gaussian, for the ratio of $3\pi^0$ events to Dalitz events in each DAQ plane in each run, relative to the average ratio over all included runs.

runs with ratios that were more than four sigma from the average. Eight outlying runs were identified. Two of these runs were found to have different spill distributions; I modified the analysis to include only spill ranges that are present in both modes. The other six runs were found to have $3\pi^0$ to Dalitz event ratios that were approximately two-thirds the average ratio. Further investigation showed that the $3\pi^0$ sample was missing one of the three DAQ planes in each of these six runs. This was due to problems during the split. These runs were removed from both modes.

After removing these runs and spills, I re-evaluated the run ratios, this time comparing the ratio in each DAQ plane (within each run) to the overall ratio. The distribution of the number of sigma away from average for each plane's ratio is shown in Figure 3. Since the sigma distribution is gaussian centered at 0 with a width of ~ 1, this plot suggests that we have eliminated all runs in which problems occurred during data-taking, tape splits, and tape migration.

MONTE CARLO

We use Monte Carlo version 6.03 (the same as was used for the V_{us} analysis [4]) to generate signal and normalization mode events. Prior to this analysis, the 832 MC initialization code did not initialize variables associated with the the Dalitz decay (such as 'pi0_slope_param,' which is the form factor parameter for the Dalitz decay), so the relevant portion of the 799 MC initialization routine were copied into the 832 routine. The photon unsmearing routine developed for version 7.00 was imported and is used to correct the resolution of the reconstructed $e^+e^-\gamma$ mass. The radiative corrections routines developed by the University of Colorado group are used in generating the $\pi^0 \to e^+e^-\gamma$ decay.

NUMBER OF EVENTS, ACCEPTANCES

Table II shows the number of events in data and MC for both $3\pi^0$ and Dalitz, and the corresponding acceptances with errors. The first two lines give the overall numbers, and below that, the events are broken into intensity ranges. The medium intensity sample includes spills which have SEM values of 3.0×10^{12} to 5.5×10^{12}, and the high intensity sample includes spills which have SEM values greater than 5.5×10^{12}. In particular, this means that run-ranges are not used as intensity ranges. Note that the sum of events in the medium and high intensity samples does not equal the total number of events; this is because some events are in the low intensity range (SEM less than 3.0×10^{12}) which is not considered separately here due to low statistics.

SYSTEMATICS

Table III is a summary of the sources of systematic errors for this analysis and an estimate for each one. For each line in the table, there is a subsection below giving more details about the source of the error and about how the estimate of the uncertainty was obtained.

Radiative Corrections

I generated signal Monte Carlo with no radiative corrections to compare to nominal MC. The acceptance increases by $(5.26 \pm 0.27)\%$ when radiative corrections are not included,

Mode	Data Events	MC Events	MC Gen	Acceptance (10^{-2})	Error (10^{-2})
$3\pi^0$	3530309	25331492	669341287	3.78454	0.00074
Dalitz	66432	273338	658870528	0.04149	0.00008
$3\pi^0$ medium	1613157	11530307	271272384	4.2505	0.0012
Dalitz medium	30843	125500	267060096	0.04699	0.00013
$3\pi^0$ high	1868668	13457397	387318016	3.4745	0.0009
Dalitz high	34565	144429	381247040	0.03788	0.00010

TABLE II: Number of events in data and Monte Carlo, and acceptances (with errors) for both modes, overall and within the medium and high intensity ranges.

Source of Systematic Error	Level of Uncertainty
Radiative Corrections	1.02%
Tracking Inefficiency	0.68%
Detector Material	0.37%
Accidentals	0.1%
Trigger Inefficiency	0.14%
Trigger 6 pre-scale	$< 0.1\%$
Form Factor	0.07%
Photon Inefficiency	0.01%
Background	$< 0.1\%$
Cut Variations	$< 0.1\%$
Monte Carlo Statistics	0.19%
Total Systematic Error	1.32%

TABLE III: Sources of systematic errors with an estimate for each uncertainty.

and the reconstructed $e^+e^-\gamma$ mass distribution is not well-modelled. Figure 4 shows that, without radiative corrections, the MC does not match the low side of the mass distribution.

The width of the reconstructed $e^+e^-\gamma$ distribution in the nominal MC matches the data quite well. The width of the mass distribution in MC with no radiative corrections is 10.33 sigma from the width of the data mass distribution. See Table IV. A more than two-sigma

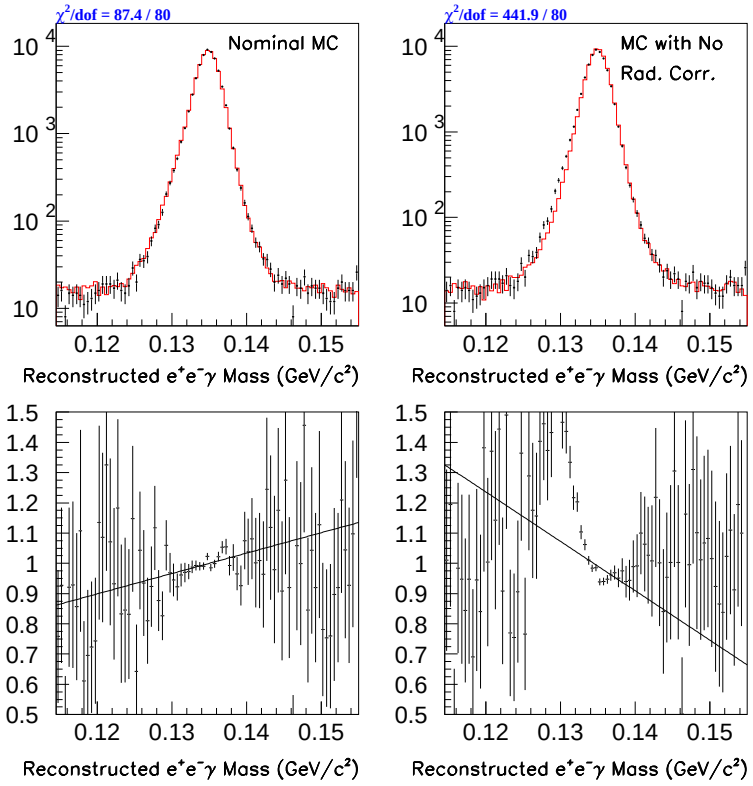

FIG. 4: The left plots show the data to nominal Monte Carlo overlay and ratio for the reconstructed $e^+e^-\gamma$ mass. The right plots are the overlay and ratio for the reconstructed $e^+e^-\gamma$ mass in data and Monte Carlo with no radiative corrections. Black dots are data; the red histogram is MC.

disagreement in the width between data and MC with no radiative corrections would be significant, so we conservatively assign a systematic error due to radiative corrections of $\frac{5.26\%}{10.33/2}$, or 1.02%.

The distribution of the number of software clusters provides a cross-check on the systematic error due to radiative corrections. The number of software clusters is affected by the real radiated photons that are generated when radiative corrections are included in the MC. Since radiative corrections also include virtual corrections, which do not affect the number of software clusters, the distribution of the number of software clusters cannot be used directly to determine a systematic error.

Figure 5 shows that overlaying this distribution from nominal Monte Carlo with data gives a χ^2 of 12.8/13; using MC with no radiative corrections gives a χ^2 of 538/13. We create a

Sample	Width of rec. $e^+e^-\gamma$ mass	Error	χ^2/dof of overlay with data	Sigma diff. from data
Data	0.0015382	5.8×10^{-6}	-	-
Nominal MC	0.0015443	3.0×10^{-6}	87.4/80	0.94
MC no rad. corr.	0.0014716	2.7×10^{-6}	441.9/80	-10.33

TABLE IV: The width of the gaussian fit to the reconstructed $e^+e^-\gamma$ mass distribution in data, nominal Monte Carlo, and Monte Carlo with no radiative corrections.

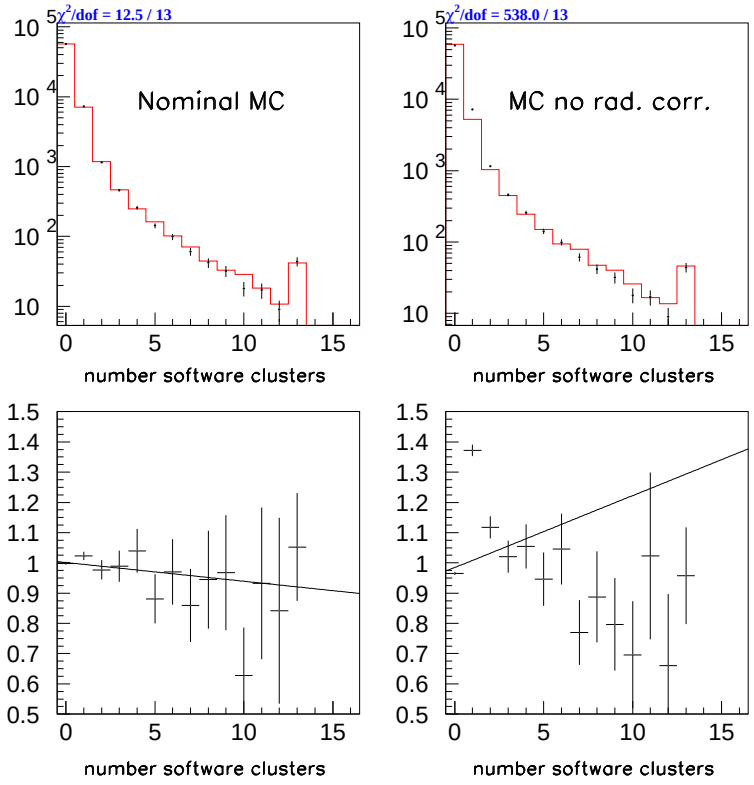

FIG. 5: The left plots show the data to nominal Monte Carlo overlay and ratio for the distribution of the number of software clusters. The right plots show the overlay and ratio for data to MC with no radiative corrections. Black dots are data and the red histogram is MC.

mixture of the two Monte Carlos (with and without radiative corrections) by combining a fraction, f, of Monte Carlo with no radiative corrections and (1-f) of nominal Monte Carlo. By varying f, we determine at what level we can detect the presence of the Monte Carlo with

no radiative corrections by monitoring the changing χ^2 to see when the combined MC no longer matches the data. When I combine 86% nominal MC with 14% MC with no radiative corrections, the χ^2 is 31.3/13. This is equivalent to more than a three sigma difference. If real radiated photons accounted for the entire 5.26% acceptance change, I would conclude that we are sensitive to changes in the acceptance due to radiative corrections at a $\sim 14\%$ level. This would give a systematic error associated with radiative corrections of $0.14 \times 5.259\% = 0.75\%$. Since virtual corrections also affect the acceptance, but not the number of software clusters, we assign a systematic error due to radiative corrections of 1.02% based on the width of the reconstructed $e^+e^-\gamma$ distribution, as described earlier in this section.

Tracking Inefficiency

Tracking inefficiency was studied for the V_{us} analysis [4] using $\pi^+\pi^-\pi^0$ events for 1997. I repeated these studies using 1999 data, separately for medium and high intensity, since tracking efficiency depends on intensity. $\pi^+\pi^-\pi^0$s were reconstructed from random accepts in trigger 4, and a large MC sample of $\pi^+\pi^-\pi^0$s was generated for comparison with these data events.

For the single-track inefficiency, η_1, the $\pi^0 \to \gamma\gamma$ is reconstructed and two hadronic clusters (corresponding to the π^+ and π^-) are required in the calorimeter. One of the hadronic clusters must match a fully-reconstructed track. There are then two possible kinematic solutions for the missing track. The position of the second hadronic cluster discriminates between these two solutions. The single track inefficiency is measured in data and in Monte Carlo, and is multiplied by 2 since we have two tracks. The MC does not fully model the inefficiency observed in data, so we need a correction equal to the difference between the data and MC inefficiencies. (This correction will lower the acceptance, since it increases the MC track inefficiency to match the data inefficiency.)

Since correlated hit losses within a drift chamber can result in no reconstructed tracks, a separate study analyzed this two-track loss, η_0. Again, we start with a reconstructed $\pi^0 \to \gamma\gamma$ and two hadronic clusters in the calorimeter. We look for events where no tracks were fully reconstructed, but where there are two track segments in either the upstream pair of drift chambers or the downstream pair. Finding two track segments in one pair of drift chambers indicates that the tracks were not reconstructed because they were both lost in

	Tracking Inefficiency Medium Intensity	Tracking Inefficiency High Intensity
Data		
$2\eta_1$	3.48%	4.90%
η_0	0.19%	0.21%
Total	3.67%	5.11%
Monte Carlo		
$2\eta_1$	2.97%	4.31%
η_0	0.05%	0.09%
Total	3.02%	4.40%
Correction	0.65%	0.72%
MC no accidentals		
$2\eta_1$	0.41%	0.41%
η_0	0.00%	0.00%
Total	0.41%	0.41%

TABLE V: Tracking inefficiencies in $\pi^+\pi^-\pi^0$ data and Monte Carlo, for both medium and high intensity. The correction applied to the acceptance is the difference between the total data inefficiency and the total MC inefficiency. The bottom section of the table gives the inefficiencies for MC events in which no accidentals were included.

the other pair of drift chambers. The two-track loss is measured in both data and MC. The difference in these measurements is added to the difference from the single-track inefficiency, and this is the total correction to the acceptance due to tracking inefficiency. Note that the total track inefficiency for events with two tracks is then $2\eta_1 + \eta_0$.

Table V shows the inefficiencies in data and Monte Carlo in the two intensity samples. The statistical errors associated with the inefficiencies are at the few percent level. Since the medium and high intensity samples are roughly equal in size, the overall tracking correction is approximately the average of the corrections in the two samples (0.68%). This entire correction is taken as a systematic error.

The remaining aspect of the tracking inefficiency is to justify that the studies done with

$\pi^+\pi^-\pi^0$s are also valid for the electron tracks that occur in the Dalitz mode. It is suspected that most of the track loss in 1999 is due to accidentals. This is verified by rerunning the MC portion of the tracking studies without accidentals; these results are shown in the bottom section of Table V. The tracking inefficiencies in MC with no accidentals are much smaller and are not intensity-dependent. A large fraction of the inefficiency ($\sim$ 85% to 90%) comes from accidentals. For more on accidentals, see the section below.

Detector Material

Turning off bremsstrahlung in the Dalitz Monte Carlo increases the acceptance by (3.67$\pm$ 0.33)%. Based on previous studies (for the V_{us} analysis [4]), the Monte Carlo models the detector material at the 10% level, so we assign a systematic error of 0.37% for this.

Accidentals

To study the effect of accidentals, we generate MC with no accidental overlays. The change in acceptance is large in both modes; it increases by (35.9 ± 0.37)% in Dalitz mode and (31.7 ± 0.06)% in $3\pi^0$ mode. Because we are taking the ratio, most of the change in acceptance cancels. The change in the ratio of branching ratios due to these changes in acceptance is $\frac{1.317}{1.359} - 1 = -0.0309$; that is, the ratio of branching ratios decreases by 3.09% if accidentals are not included in the MC.

Since this change in the ratio of branching ratios is mainly due to the presence of tracks in the signal mode, we can use the drift chamber sum-of-distances (SOD) distributions for the tracks to measure our sensitivity to changes in the acceptance due to accidentals. Figure 6 shows the SOD distribution in data, nominal MC, and MC with no accidentals. The overlay between data and MC without accidentals shows extremely poor agreement. The agreement between data and nominal MC is much better, but it is significantly less-than-perfect. Because the χ^2 for data to nominal MC is rather large, it cannot be used in the MC mixing technique like it was for the systematic error due to radiative corrections.

However, since accidentals contribute almost entirely to the low SODs, we can use the fraction of events in the SOD distribution below -0.2 mm in place of the χ^2. This quantity is well-modelled in nominal MC; in MC, this fraction is within one sigma of the fraction in

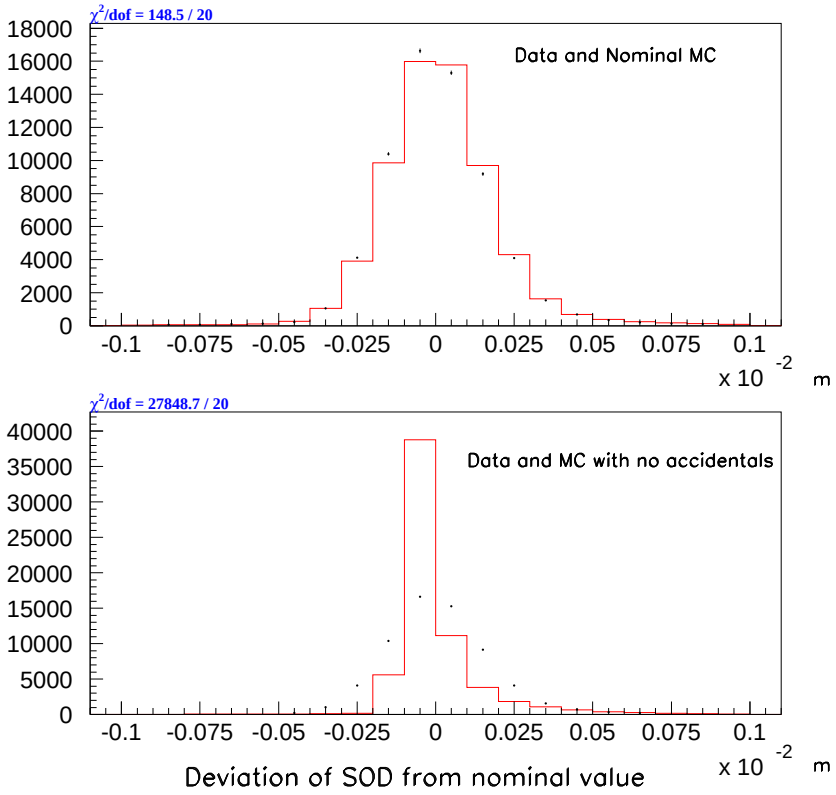

FIG. 6: Data to Monte Carlo overlays of drift chamber sum-of-distance (SOD) distributions for tracks in DC1X. The top plot is nominal MC and the bottom plot is MC without accidentals. The black dots are data and the red histogram is MC. Deviation between SOD and cell spacing is shown, so zero deviation means SOD=6.35mm, and negative deviations are low SODs.

data. The fraction of low SOD events in MC with no accidentals differs from the fraction in data by 68 sigma; see Table VI. We create a mixture of MC with and without accidentals and monitor the change in this low-SOD fraction to see how much MC with no accidentals must be present to produce a significant ($\sim$ 3 sigma) difference in this fraction between the mixed MC and data. 2.5% MC with no accidental overlays is needed to reach this threshold. See Table VI and Figure 7. This means that we are sensitive to changes in the ratio of branching ratios (due to accidentals) greater than $3.09\% \times 0.025 = 0.08\%$, so the systematic error associated with accidentals is 0.08%. This is a measure of our sensitivity to accidentals in the charged part of the signal mode.

Because we also have one more photon in the normalization mode than in the signal

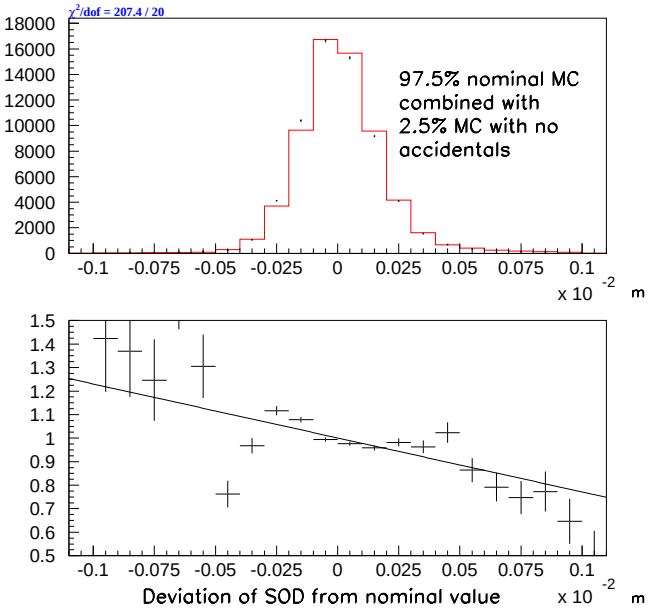

FIG. 7: Data to MC overlay of drift chamber sum-of-distance (SOD) distributions for tracks in DC1X. The MC is 97.5% nominal and 2.5% without accidentals. The black dots are data and the red histogram is MC. Deviation between SOD and cell spacing is shown, so zero deviation means SOD=6.35mm, and negative deviations are low SODs.

mode, we are also sensitive to accidentals in the neutral parts of the two decays. Comparing the distribution of the number of software clusters for $3\pi^0$ MC events with and without accidentals gives a measure of this part of our sensitivity to accidentals. Using 98% nominal MC with 2% MC with no accidentals gives a very significant mismatch with data in the distribution of the number of software clusters. For the neutral parts of the decays, we are sensitive to changes in the ratio of branching ratios (due to accidentals) greater than $3.09\% \times 0.02 = 0.06\%$. Combining this systematic error with the systematic error from our sensitivity to accidentals in the charged part of the signal mode gives a total systematic error due to accidentals of 0.1%.

Trigger Inefficiency

Since the two modes come from two different triggers, we need to measure how well we know the relative trigger efficiency. The $3\pi^0$s come from trigger 6, and the Dalitz events

Sample	Fraction Dev Sod $< -.2$mm	Error	Sigma Diff From Data
Data	0.1169	0.0012	-
Nominal MC	0.1156	0.0006	0.90
MC no accid.	0.0282	0.0004	67.99
MC: 97.5% nom and 2.5% no accid.	0.1126	0.0006	3.06

TABLE VI: The fraction of events (and the error) whose deviation of SOD from the nominal value (6.35 mm) is less than -.2 mm. The last column gives the difference in this low-sod fraction between data and MC for nominal MC, MC with no accidentals, and a combination of the two Monte Carlos.

come from trigger 14. To determine the level of trigger inefficiency, I take random accepts from trigger 6 and run them through my Dalitz analysis. The fraction of the events that reconstruct as Dalitz decays but do not show up in trigger 14 is the rate of trigger inefficiency. I find 207 random accepts that pass all my Dalitz cuts, and all 207 are in trigger 14. I find 716 events that pass all cuts except the cell separation cut, and 1 of these is not in trigger 14. This inefficiency of $\frac{1}{716} = 0.0014$ is applied to the Dalitz acceptance as a correction, and the entire correction of 0.14% is taken as a systematic error.

Trigger 6 Prescale

Based on past trigger studies, we estimate that this systematic error will be less than 0.1%. For the final result, we will reconstruct $3\pi^0$s in trigger 5 and measure the rate of events that pass all cuts but are not in trigger 6.

Form Factor

The amplitude for the π^0_d decay, $\pi^0 \to e^+e^-\gamma$, contains a form factor, F(x), at the $\pi^0\gamma\gamma$ vertex (where $x = (m_{ee}/m_{\pi^0})^2$). The linear expansion of F(x) is 1+ax; the PDG value for the parameter a is 0.032 ± 0.004. I generated MC with the nominal value of this parameter, as well as with a value of 0.0 (eight sigma below nominal) and a value of 0.064 (eight sigma above nominal). Changing the form factor parameter up or down by eight sigma has only a

small affect on the acceptance; it differs from nominal by approximately $(0.6 \pm 0.3)\%$, giving a systematic error of 0.07%.

Photon Inefficiency

In the V_{us} analysis [4], the effect of the photon cluster shape requirement (shape χ^2) was studied by removing this cut in the $\Gamma_{000}/\Gamma_{Ke3}$ analysis. Removing the cut resulted in a change of 0.05% in the ratio, which was taken as a systematic uncertainty. In this analysis, there is only a one-photon difference between the numerator and denominator of the ratio of branching ratios (five photons in the signal mode and six photons in the normalization mode). The uncertainty in $\frac{B(K_L \to 3\pi^0_d)}{B(K_L \to 3\pi^0)}$ is then 1/6 of the one found in V_{us}, or, $\sim$0.01%.

Background

$K_L \to 3\pi^0$, with one photon converting to an e^+e^- pair at the vacuum window is the main source of background. To study this, $3\pi^0$ Monte Carlo events were generated in trigger 14 and reconstructed with the Dalitz analysis. Figure 8 shows the distribution of reconstructed vertex position for the conversion events, zoomed in to the region around the vacuum window at 159 meters.

We generated half as many $3\pi^0$s for this background study as we did for the nominal $3\pi^0$ analysis; since the nominal analysis only kept $\frac{1}{50}$ events due to the trigger 6 prescale of 5 along with a prescale of ten in my crunch, we generated a factor of 25 more $3\pi^0$ events for the background study. (This is because we need to know, not only how many background events this sample produced, but also how many $3\pi^0$ events it would have produced had it gone through trigger 6 and the nominal $3\pi^0$ analysis. By generating $25\times$ as many $3\pi^0$s for the background study, this latter number is just half the number of $3\pi^0$s we reconstruct in our nominal $3\pi^0$ Monte Carlo (25331492/2 = 12665746 events), since the underlying samples sizes differ by a factor of two.)

Only seven background events remain after all cuts. Since we reconstructed 3,530,309 $3\pi^0$ events in data, and 12,665,746 in MC, the number of background events expected in data is $7 \times \frac{3530309}{12665746} = 2.0$ events. This represents $\frac{2.0}{66432} = 3 \times 10^{-5}$, or a 0.003% background, and we take this as a systematic error.

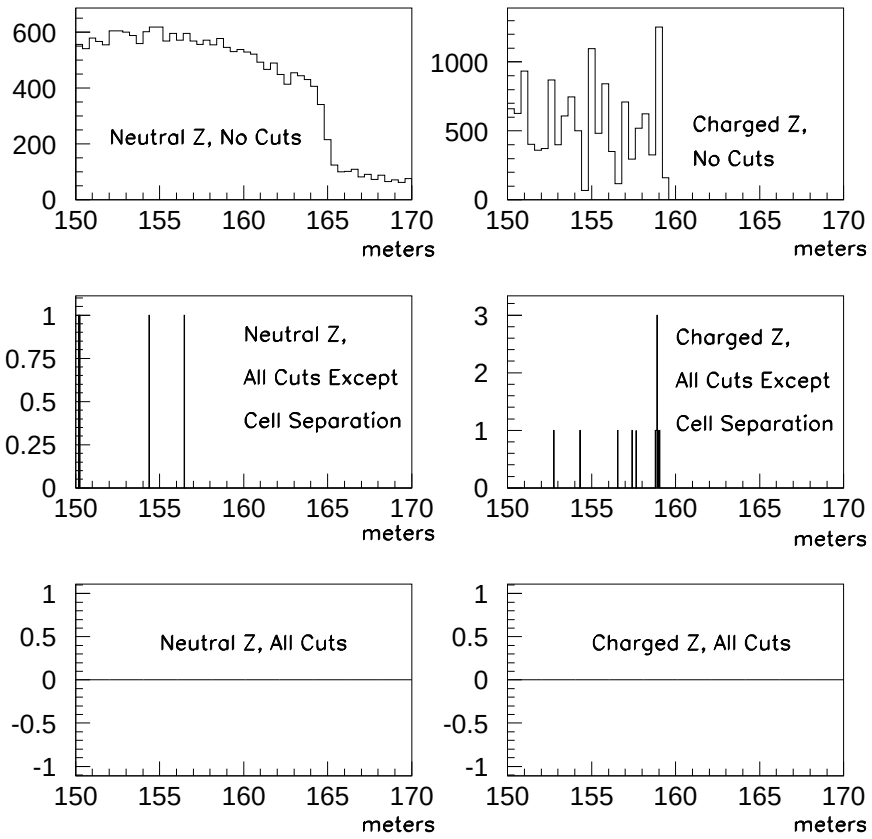

FIG. 8: The reconstructed vertex position of events with a photon conversion, focusing on the region near the vacuum window (at 159 m). The plots on the left show the reconstructed vertex position based on the neutral photons that formed the $2\pi^0 s$. The plots on the right are the reconstructed vertex position based on the vertex of the two tracks. The top plot is before cuts, the middle plot is after all cuts except the cell separation requirement, and the bottom plot is after all cuts. In the top-right and middle-right plots, the spike at the vacuum window is visible. Note that seven events remain after all cuts, although none of them are near the vacuum window.

Cut Variations

Plotting data to Monte Carlo overlays for each variable shows that the simulation models the physics very well. Figure 9 shows the reconstructed vertex position distributions in both Dalitz and $3\pi^0$ modes. There is no significant slope in the ratio of data to Monte Carlo z-positions in either mode. Figure 10 shows the cell separation distribution for the two tracks

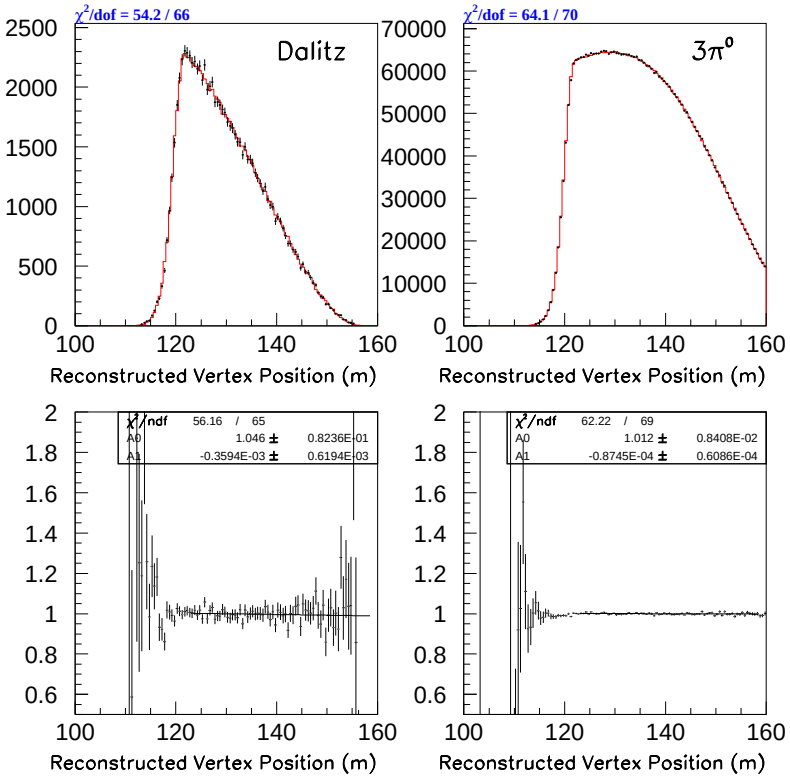

FIG. 9: The reconstructed kaon z-vertex for both modes, after all cuts except the z cut. The black dots are data and the red histogram is Monte Carlo.

in Dalitz mode. The left plot show the distribution after all cuts except the cell separation cut; the right plot shows the distribution after making the additional requirement that the cell separation be greater than 3 (cells). Most of the disagreement is in the first bin, at a cell separation of zero. It is not surprising that it is difficult to simulate cases in which the two tracks are so close together as to be within the same cell in the drift chamber.

Systematics associated with cuts on variables are studied by varying each cut and seeing what happens to the $\frac{B(\pi^0 \to e^+e^-\gamma)}{B(\pi^0 \to \gamma\gamma)}$. For variables on which a requirement exists in both modes, a large fraction of any data-Monte Carlo disagreements should cancel in the ratio, and we find this to be the case when cuts are varied. For variables that only exist in Dalitz mode, no such cancellation will occur, so systematic errors arise from any disagreement between data and Monte Carlo. The cuts on these Dalitz-only quantities are varied, and no significant changes are observed in $\frac{B(\pi^0 \to e^+e^-\gamma)}{B(\pi^0 \to \gamma\gamma)}$. Based on this, we estimate that our sensitivity to changes in the acceptance due to the selection criteria is small, $< 0.1\%$.

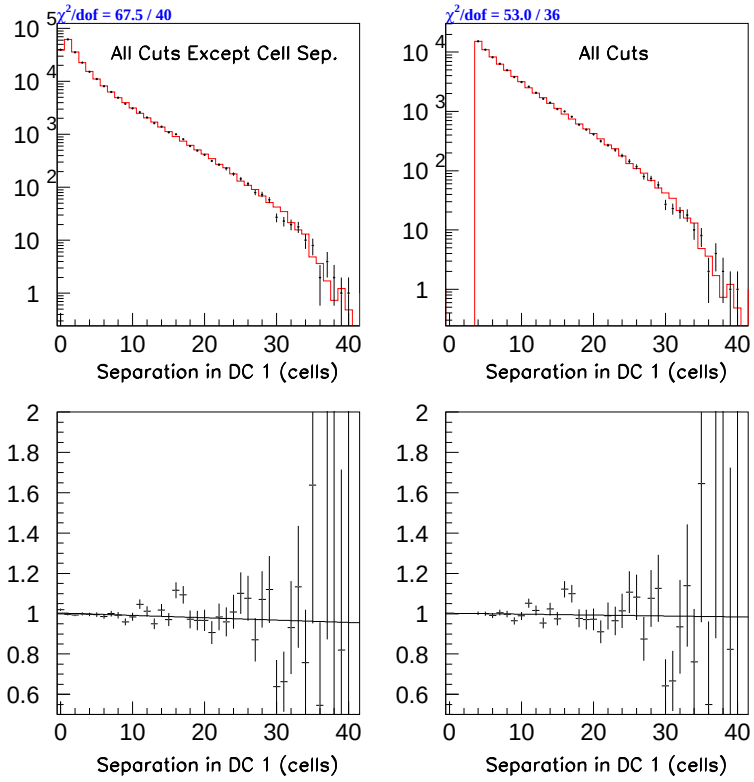

FIG. 10: The reconstructed cell separation for the two tracks in Dalitz mode. The left plot is after all cuts except the cell separation cut, and the right is after all cuts. Most of the disagreement between data and Monte Carlo is in the first bin, at a cell separation of 0.

Monte Carlo Statistics

The error on the ratio of acceptances, which is 0.19%, is taken as the error from MC statistics. This number can be reduced for the final result by generating a larger Monte Carlo sample for Dalitz mode (since this mode currently limits the error on the ratio of acceptances).

CROSS-CHECKS

We have several ways to cross-check our result, some of which have been done and some of which are in progress. These include calculating the ratio of branching ratios within each intensity range, for each value of the cell separation, for each run, for inbends and outbends,

Sample	$B(\pi^0 \to e^+e^-\gamma)/B(\pi^0 \to \gamma\gamma)$	Stat. Error (Data and MC)
Medium Intensity	1.1621	0.0074
High Intensity	1.1408	0.0069
Weighted Average	1.1506	0.0050
Overall	1.1539	0.0050

TABLE VII: The intensity dependence of the ratio of branching ratios. Using (data and MC) statistical errors only, we compute the weighted average of the results in the two intensity samples. The overall result is included in the bottom line for comparison.

and for the two magnet polarities.

Intensity Dependence

The ratio of branching ratios, $\frac{B(\pi^0 \to e^+e^-\gamma)}{B(\pi^0 \to \gamma\gamma)}$ is calculated independently in the medium and high intensity samples. The correction for the tracking inefficiency is applied separately to the two samples; the medium intensity correction to the Dalitz acceptance is 0.9935 and the high intensity correction is 0.9928. The correction due to the trigger inefficiency is the same for both samples. The results are shown in Table VII.

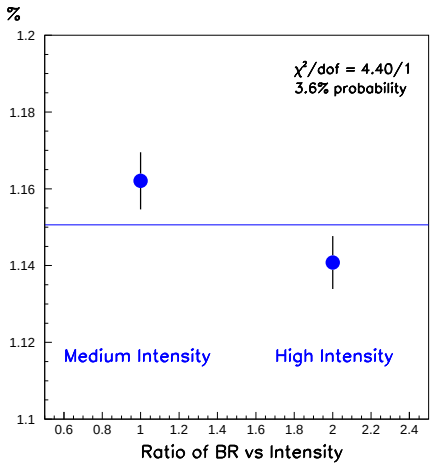

FIG. 11: The points are the ratio of branching ratios in each intensity sample, and the line is the weighted average.

Using the weighted average and the errors, we compute χ^2 for one degree of freedom of 4.40. This χ^2 indicates a 3.6% probability that the results from the two intensity samples are consistent with each other within statistical errors. This fit is shown in Figure 11.

Cell Separation Dependence

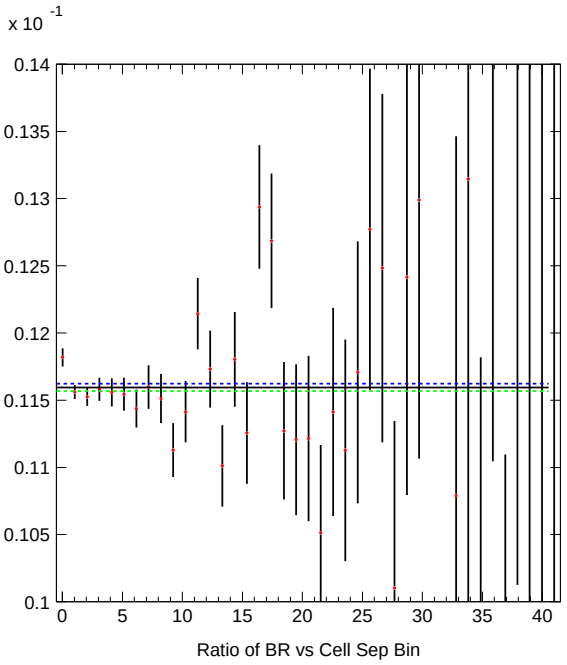

FIG. 12: The ratio of branching ratios vs cell separation. The Dalitz events (both data and reconstructed MC events) that contribute to the answer in each bin are the events which have a minimum cell separation equal to the bin number. For example, the events in the cell separation = 0 bin all have a minimum cell separation of exactly 0.

Because tracks with a small opening angle are not well-simulated in the Monte Carlo, we require that the tracks be more than 3 cells apart in the first two drift chambers. We now verify that the ratio of branching ratios is not changing significantly in the vicinity of our cut. The number of reconstructed Dalitz events in each bin of cell separation in both data and MC are used to compute the ratio of branching ratios for each value of cell separation. (We use the overall number of reconstructed $3\pi^0$ events in data and MC, as well as the overall number of generated events in both modes since we do not currently have a measure of the number of generated events for each value of the cell separation.)

Figure 12 shows the ratio of branching ratios as a function of cell separation. Tracks with a minimum cell separation of zero are very poorly simulated; beyond zero cell separation, the ratio of branching ratios is fairly flat. Fitting the points to a line using all the bins gives a χ^2/dof of 64.4/38; omitting the zero cell separation bin significantly improves the χ^2/dof to 53.7/37.

Run Dependence

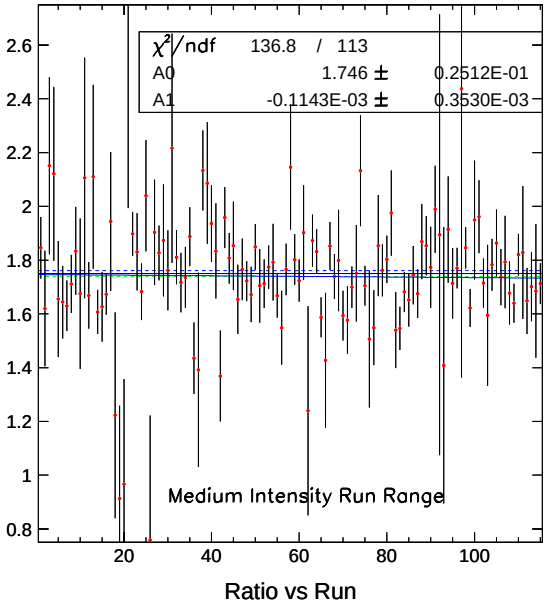

FIG. 13: The ratio of branching ratios vs run, for 'medium-intensity' runs, which are defined as runs 13670 through 14104. Note that this does not exactly correspond to the medium intensity sample, since events for the medium intensity sample are selected on a spill-by-spill basis. Only runs which have a non-zero number of events in them are included.

Recall that, before making any cuts, we checked the data sample integrity by looking at the ratio of the number of $3\pi^0$ events to the number of Dalitz events in each DAQ plane in each run, and comparing that ratio to the ratio over all runs. We used the statistical error within each run to determine, for each individual ratio, the number of sigma away from the overall average ratio.

A similar check is performed after the analysis for events passing all cuts. For each run

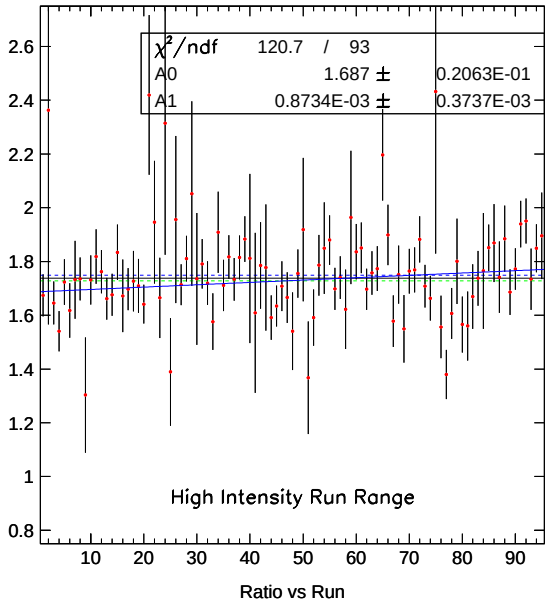

FIG. 14: The ratio of branching ratios vs run, for 'high-intensity' runs, which are defined as runs 14105 through 14523. Note that this does not exactly correspond to the high intensity sample, since events for the high intensity sample are selected on a spill-by-spill basis. Only runs which have a non-zero number of events in them are included.

that has a non-zero number of events, we compute the ratio $(\frac{\text{ndaldata}}{\text{n3p0data}} * \frac{\text{n3p0mcrec}}{\text{ndalmcrec}})$. We compute this number (with an error based on data and MC statistics) in lieu of the ratio of branching ratios in each run because currently there is no measure of the number of generated events in our energy and z ranges on a run-by-run basis. This number is also computed across all runs for comparison.

Due to the intensity-dependence of the above ratio, it is appropriate to separate out the two intensities. During data-taking, the intensity was increased at run 14105 for high intensity running through the end of the 99 runs. We break the run range into a 'medium intensity' run range (runs 13670-14104) and a 'high intensity' run range (runs 14105-14523). (Note that this is not how the previously described medium and high intensity samples are selected; events are put into one of those samples based on a spill-by-spill SEM value.) This is imperfect since some runs in the former range were high intensity tests, and some spills in one intensity run range have an actual intensity that would put them in the other range. The plots in Figure 13 and Figure 14 show the ratios for each run in the. The fits agree at

around the two-sigma level.

Inbends vs Outbends

This study is in progress.

Magnet Polarity

This study is in progress.

[1] M. Schardt et al., Phys. Rev. D **23** (1981).

[2] N. Samios, Phys. Rev. **121** (1961).

[3] Y. Budagov et al., JETP **11** (1960).

[4] T. Alexopoulos et al., Phys. Rev. D **70** (2004).